36 *Chem. Mater.* **2010,** *22,* 36–46
DOI:10.1021/cm900183v

CHEMISTRY OF MATERIALS
Article

Thermodynamic Modeling of Hydroxyapatite Crystallization with Biomimetic Precursor Design Considerations

Christina Mossaad, Matthew Starr, Swanand Patil, and Richard E. Riman*

Department of Materials Science and Engineering, Rutgers, The State University of New Jersey, 607 Taylor Road, Piscataway, New Jersey 08854

Received January 20, 2009. Revised Manuscript Received August 25, 2009

The objective of this paper is to present a hydroxyapatite synthesis biomimetic precursor paradigm and evaluate four precursor systems against its criteria. Thermodynamic modeling was used as a method of evaluation. The system that best fit the paradigm was experimentally validated by synthesizing inorganic powders over a range of reaction conditions and characterizing the reaction products through X-ray diffraction. The $Ca(C_2H_3O_2)_2-K_3PO_4-H_2O$ system was found to best fit the paradigm and was effective in synthesizing hydroxyapatite as predicted by the yield diagram. On the basis of the findings of this diagram and its validation, it appears that thermodynamics largely governs the synthesis of hydroxyapatite in all these systems, making these equilibrium diagrams valuable for future research on hydroxyapatite crystallization.

1. Introduction

Hydroxyapatite ($Ca_5(PO_4)_3OH$ or $Ca_{10}(PO_4)_6(OH)_2$) is an inorganic material that has a variety of potential applications in modern science. It has been used in chromatography,[1] corrosion resistant materials,[2] drug delivery,[3] and most notably bone implant coatings[4] and composites[5] due to its osteoconductive nature. There has been a shift toward adapting hydroxyapatite synthesis techniques to more closely resemble how it is made naturally in the human body, or in other words, a biomimetic process. However, the majority of synthetic methods in the literature cannot be classified as biomimetic processes even though they may yield biomimetic materials because the precursors and other reaction conditions for synthesis are not observed in nature. Many variations of a definition of biomimetic materials have been postulated involving the use of simulated body fluid, proteins, or collagen to produce hydroxyapatite, but these fail to address the flaws in the starting chemical precursors used in a biomimetic process.[6−8]

While these perspectives on biomimesis (the art of mimicking natural phenomena) are important, the precursor design is no less crucial in finding a true biomimetic system that can produce hydroxyapatite in high yield. The vision of a biomimetic crystallization paradigm, or model, for the creation of a less harsh hydroxyapatite synthesis method necessitates a critical look at the reaction conditions under which the mineral is formed naturally in the body. Average healthy body conditions are 37 °C, pH of 7.4, which produce 10−40 nm hydroxyapatite crystals in hard tissue depending on mechanical loading, health, and nutrition.[9−11] In contrast, current hydroxyapatite synthesis methods utilize reaction conditions from 25 to 1200 °C, pH of 8−12 (with or without a pH agent modification), producing particles anywhere from 15 nm to 2 μm.[12−33]

(1) Lawson, M. A.; Xia, Z. *Bone* **2006**, *38*(3), S1, 55.
(2) Garcia, C.; Cere, S.; et al. *J. Non-Cryst. Solids* **2004**, *348*, 218.
(3) Ginebra, M. P.; Traykova, T.; et al. *J. Controlled Release* **2006**, *113*(2), 102.
(4) Kuo, M. C.; Yen, S. K. *Mater. Sci. Eng. C* **2002**, *20*(1−2), 153.
(5) Wei, G.; Ma, P. X. *Biomaterials* **2004**, *25*, 4749.
(6) Landi, E.; Tampieri, A.; Celotti, G.; Langenati, R.; Sandri, M.; Sprio, S. *Biomaterials* **2005**, *26*(16), 2835.
(7) Kikuchi, M.; Ikoma, T.; Itoh, S; Matsumoto, H. N.; Koyama, Y.; Takakuda, K.; Shinomiya, K.; Tanaka, J. *Compos. Sci. Technol.* **2004**, *64*(6), 819.
(8) Ma, P. X. *Adv. Drug Delivery Rev.* **2008**, *60*(2), 184.
(9) Ilich, J. Z.; Kerstetter, J. E. *J. Am. Coll. Nutr.* **2000**, *19*(6), 715.
(10) Silver, F. H.; Freeman, J. W.; et al. *J. Biomech.* **2003**, *36*(10), 1529.
(11) Katti, K. S. *Colloids Surf., B* **2004**, *39*(3), 133.
(12) Suchanek, W. L.; Shuk, P.; et al. *Biomaterials* **2002**, *23*(3), 699.
(13) Shu, C.; Yanwei, W.; Hong, L.; Zhengzheng, P.; Kangde, Y. *Ceram. Int.* **2005**, *31*(1), 135.
(14) Liao, Q.; Xu, G.; Yin, G.; Zhou, D.; Zheng, C.; Li, X. *J. Funct. Mater.* **2002**, *33*(3), 38.
(15) Cao, M.; Wang, Y.; Guo, C.; Qi, Y.; Hu, C. *Langmuir* **2004**, *20*(11), 4784.
(16) Yan, L.; Li, Y.; Deng, Z.; Zhuang, J.; Sun, X. *Int. J. Inorg. Mater.* **2001**, *3*(7), 633.
(17) Liu, J.; Ye, X.; Wang, H.; Zhu, M.; Wang, B.; Yan, H. *Ceram. Int.* **2003**, *29*(6), 629.
(18) Kim, I.; Kumta, P. N. *Mater. Sci. Eng. B* **2004**, *111*(2−3), 232.
(19) Kuriakose, T. A.; Kalkura, S. N.; Palanichamy, M.; Arivuoli, D.; Dierks, K.; Bocelli, G.; Betzel, C. *J. Cryst. Growth* **2004**, *263*(1−4), 517.
(20) Ramanan, S. R.; Venkatesh, R. *Mater. Lett.* **2004**, *58*(26), 3320.
(21) Grandjean-Laquerriere, A.; Laquerriere, P.; et al. *Biomaterials* **2006**, *27*(17), 3195.
(22) Li-yun, C.; Chuan-bo, Z.; Jian-feng, H. *Mater. Lett.* **2005**, *59* (14−15), 1902.
(23) Afshar, A.; Ghorbani, M.; Ehsani, N.; Saeri, M. R.; Sorrell, C. C. *Mater. Des.* **2003**, *24*(3), 197.
(24) Zhang, H.; Wang, Y.; Yan, Y.; Li, S. *Ceram. Int.* **2003**, *29*, 413.
(25) Wang, A.; Liu, D.; et al. *Mater. Sci. Eng. C* **2007**, *27*(4), 865.
(26) Liu, C.; Huang, Y.; et al. *Biomaterials* **2001**, *22*, 301.
(27) Saeri, M. R.; Afshar, A.; Ghorbani, M.; Ehsani, N.; Sorrell, C. C. *Mater. Lett.* **2003**, *57*(24−25), 4064.
(28) Rendón-Angeles, J. C.; Yanagisawa, K.; Ishizawa, N.; Oishi, S. *J. Solid State Chem.* **2000**, *151*(1), 65.
(29) Yoshimura, M.; Sujaridworakun, P.; Koh, F.; Fujiwara, T.; Pongkao, D.; Ahniyaz, A. *Mater. Sci. Eng. C* **2004**, *24*(4), 521.
(30) Jinawath, S.; Polchai, D.; et al. *Mater. Sci Eng. C* **2002**, *22*(1), 35.
(31) Zhang, L.-J.; Feng, X.-S.; et al. *Mater. Lett.* **2004**, *58*(5), 719.
(32) Tas, A. C. *Biomaterials* **2000**, *21*, 1429.
(33) Bayraktar, D.; Tas, A. C. *J. Eur. Ceram. Soc.* **1999**, *19*, 2573.

Published on Web 12/02/2009

A paradigm biomimetic precursor hydroxyapatite synthesis system would precipitate at or below 37 °C, relatively constant neutral pH (7−7.8), in high enough yield (> 1 g per 100 mL reaction) for industrial applications in less than 4 h using precursors that do not leave toxic ions in solution. The ions left in solution should either be abundant in the body or metabolizable so minimum washing of the powder would be necessary prior to application. The pH could be controlled through the use of benign biological buffers or through the proper precursor choice. A synthesis time under 4 h is desirable because longer than this is not optimal for industrial scale up, could compromise aseptic processing in the manufacture of implant composites, and would not be optimal for surgical settings. A paradigm biomimetic precursor system could also mineralize live tissue during operative surgical procedures, an application that emphasizes the need for a short time and benign processing condition with high enough yield to produce a positive cellular response but does not require specialized equipment or manipulation or washing after crystallization. A chemically robust system is one that does not entirely depend on input reactant stoichiometry (Ca/P range 0.5−4 and still produces HA) . Additionally, having no dependency on the degree of mixing in both industrial and surgical venues would more easily yield consistent results, reducing concern of under/over mixing.

It is clear that current hydroxyapatite synthesis methods do not meet all these requirements in various ways. Methods commonly employed include mechanochemical,[12,13] hydrothermal,[14−17] sol−gel,[18−21] precipitation,[22−27] phase transition,[28−30] and simulated body fluid[31−33] crystallizations. The most widely used method is hydrothermal synthesis, which typically requires a long reaction time (> 24 h), high temperatures (50−300 °C), and high pressures (> 4 atm) to produce hydroxyapatite, which are completely incompatible processing conditions for biological systems. Hydrothermal synthesis can be adapted to precipitate at room temperature and atmospheric pressure, but extreme pH is required, also prompting biological protein denaturation and degradation. Mechanochemical synthesis requires the use of high shear rates that would tear and break down any soft biological matter present. Sol−gel synthesis requires a solid state thermal treatment at high temperatures (> 900 °C) to crystallize precursor powder, conditions yet again provoking breakdown of biological matter. The phase transition approach often requires the use of high pH (> 8) and long processing times (> 24 h) and high temperatures (> 60 °C) to attain complete conversion. The use of simulated body fluid has become the most popular method of biomimesis; although the process is biomimetic, it has a fatal flaw in the innate long reaction time (> 7 days) and low yield (≪ 0.1 g per 100 mL reaction), not conducive to application outside of research. Additionally, these methods often employ additional additives such as chelating agents and surfactants, which are necessary to remove prior to any biological exposure because of their toxicity.

The empirical, nonpredictive approaches used for hydroxyapatite synthesis have an opportunity for improvement through the use of thermodynamic modeling. Thermodynamic modeling has previously been used in designing successful synthesis approaches in lead titanate[34,35] and perovskites.[36] By modeling hydroxyapatite solution synthesis, simple precursor inflows can be designed into the system and secondary reaction additives such as pH agents, surfactants, and chelating agents and their effects can be eliminated. It will also help explore modifications to systems in the literature so they can better fit the biomimetic precursor paradigm. Many calcium and phosphate precursor combinations have been used in solution precipitation of hydroxyapatite; however, many of the individual precursors can be eliminated on the basis of chemistry and their failure to fit the biomimetic precursor paradigm. Ions that are the most prevalent in human blood plasma are Na^+, Cl^-, and K^+ (142, 103, and 5 mmol/dm^3, respectively).[37] Precursor design should take this into account, eliminating the use of iodides, hydroxides, nitrates, and fluorides, to name a few.

Three precursor systems that are widely used in literature to synthesize hydroxyapatite via solution precipitation at room temperature are $CaCl_2$−Na_3PO_4,[38] $CaCl_2$−K_2HPO_4,[39−42] and $Ca(OH)_2$−H_3PO_4.[43−45] All have experimentally used a caustic agent to maintain a pH above 9 throughout the reaction, but through the use of thermodynamic modeling, it may be possible to find reaction conditions that adhere to the biomimetic precursor paradigm. Following this paradigm further, this analysis will also omit surfactants, chelating agents, and other additives typically used for the above referenced works but not found in biological systems. Excluding these components and their potential thermodynamic effects also allows comparisons between the individual precursor systems. The $CaCl_2$ systems give information about how the precursor interacts with two different phosphate sources while the $CaCl_2$−Na_3PO_4 and $Ca(OH)_2$−H_3PO_4 systems may show the effects of using an orthophosphate source. In addition to these previously published chemistries, the $Ca(C_2H_3O_2)_2$−K_3PO_4 system models will be presented because it has not previously been investigated experimentally in the literature and will give additional comparisons for an orthophosphate model (they are analogous to Na_3PO_4) and its interactions with a highly

(34) Cho, S.-B.; Noh, J.-S.; et al. *J. Eur. Ceram. Soc.* **2003**, *23*(13), 2323.
(35) Lencka, M. M.; Riman, R. E. *J. Am. Ceram. Soc.* **1993**, *76*(10), 2649.
(36) Lencka, M. M.; Riman, R. E. *Ferroelectrics* **1994**, *151*(1−4), P1 159.
(37) Kokubo, T.; Kushitani, H.; Sakka, S.; Kitsugi, T.; Yamamuro, T. *J. Biomed. Mater. Res.* **1990**, *24*, 721.
(38) Liu, Y.; Hou, D.; Wang, G. *Mater. Chem. Phys.* **2004**, *86*, 69.
(39) Wang, Y.; Zhang, S.; et al. *Mater. Lett.* **2006**, *60*(12), 1484.
(40) Wang, F.; Li, M.-S.; et al. *Mater. Chem. Phys.* **2006**, *95*(1), 145.
(41) Chou, Y.-F.; Chiou, W.-A.; et al. *Biomaterials* **2004**, *25*, 5323.
(42) Feng, W.; Mu-Sen, L.; Yu-Peng, L.; Sheng-Song, G. *J. Mater. Sci.* **2005**, *40*, 2073.
(43) Roeder, R. K.; Converse, G. L.; et al. *J. Am. Ceram. Soc.* **2006**, *89*(7), 2096.
(44) Mostafa, N. Y. *Mater. Chem. Phys.* **2005**, *94*, 333.
(45) Kumar, R.; Prakash, K. H.; Cheang, P.; Khor, K. A. *Langmuir* **2004**, *20*(13), 5196.

Table 1. Computed Phase Equilibrium Survey for Ca−P Precursor Systems Considered for the Biomimetic Precursor Paradigm[a]

precursor (pH)	K_2HPO_4 (9.00)	H_3PO_4 (1.32)	Na_3PO_4/K_3PO_4 (12.13/12.24)
$CaCl_2$ (6.73)	N	N	H
$Ca(OH)_2$ (12.39)	H	H	H
$Ca(C_2H_3O_2)_2$ (8.92)	N	N	H

[a] Fixed conditions (Ca/P = 1.67, 0.5 *m* Ca-precursor and 0.3 *m* P-precursor solutions used for all computed equilibria (post-mixing concentrations) and 25 °C). H denotes that hydroxyapatite is the dominant phase in the equilibrium diagram, and N indicates hydroxyapatite was not dominant. Predicted pH of the respective single component Ca- or P-precursor is at the same bulk concentration as the mixed Ca−P precursor solution

soluble calcium precursor. Acetates are not native to human blood plasma; however, they are a natural metabolite of alcohol found in the bloodstream, so it is considered to fit the biomimetic precursor paradigm as well. Precursor systems that were modeled are shown in Table 1. The aqueous equilibrium pHs of the precursor solutions also show the trend in forming hydroxyapatite over other phases based on chemical selection. At least one basic component is necessary to form hydroxyapatite, as pH typically drops during crystallization due to consumption of hydroxyl ions in solution. The use of a basic solution does not fit the biomimetic precursor paradigm requirements, but a fast reaction that produces a neutral pH after 4 h could still be promising.

Current methods of solution precipitation of hydroxyapatite employ harsh precursors and conditions that limit their true biomimetic qualities. The objective of this paper is to investigate the thermodynamic models of these systems and how they may be exploited to improve hydroxyapatite solution synthesis methods. The biomimetic precursor paradigm has been outlined to set guidelines for precursor solution design. Four hydroxyapatite synthesis systems will be thermodynamically modeled to evaluate their biomimetic potential. One or more these four systems will be chosen for experimental validation based on the results of the thermodynamic modeling and its fit with the biomimetic precursor paradigm. It is hypothesized that if thermodynamics govern the solution synthesis methods of hydroxyapatite, then the proposed simulation approach will prove effective in promoting biomimetic process design.

2. Thermodynamic Computations

2.1. Design. Thermodynamic modeling methods used in this work have been previously described in detail.[46] The focus of these models, simulated using the OLI Stream Analyzer 2.0, will be to describe the relevant simulations and their relation to the biomimetic precursor paradigm proposed. The thermodynamic databases that were specified for these simulations were the public, geothermal, and ceramic databases within the stream analyzer 2.0 from OLI systems, Inc.[47]

(46) Riman, R.; Suchanek, W.; et al. *Ann. Chim. Sci. Mater.* **2002** *27*(6), 15.
(47) http://www.olisystems.com

In the thermodynamic design of a biomimetic system, the main variable parameters that impact the model are related to precursor selection, stoichiometry, and temperature, all which affect pH. Temperature for modeling was fixed at 25 °C, while the titrants used in the chemical stability diagrams were chosen as HNO_3 and KOH, which are not biomimetic, but acidic and basic inflows are necessary to generate this model, but not needed for real experimentation. Precursor inflows were chosen and fixed (other than where noted) at 0.5 *m* calcium and 0.3 *m* phosphate to model the systems at a relatively concentrated reaction for high yield, but maintaining stoichiometric proportions of Ca/P = 1.67. A summary of the computations for the various precursor systems is shown in Table 1. Precursor dependent equilibrium reactions and speciation that take place in the synthesis of hydroxyapatite are presented in Table 2. All aqueous and solid species are labeled with an (aq) or an (s), while the ionic species show their corresponding charge.

Four types of diagrams were used to evaluate the four precursor systems and their potential for the biomimetic precursor paradigm. These diagrams were namely (a) stability (b) yield (c) temperature survey and (d) composition survey diagrams. For diagrams, (a) and (b) the shaded region indicates a 99% yield of hydroxyapatite, and the incipient precipitation boundary of hydroxyapatite is shown with a solid line. Any aqueous or ionic species present is denoted with a dotted line, while secondary phase fields are shown with a dashed or dashed-dotted line.

The stability diagram shown in Figures 1−4 in position (a) correlates equilibrium pH versus log molal concentration ratio (Ca/P = 1.67), which is effective in showing how equilibrium variable pH affects phase stability at a fixed inflow precursor ratio. Yield is also shown with a shaded region on the diagram for a single selected phase, which in this case is hydroxyapatite.

The yield diagram shown in Figures 1−4 in position (b) shows phase fields produced at different precursor inflow ratios of phosphate versus calcium in molal concentrations at a fixed temperature (25 °C). The shaded region indicates a 99% yield of hydroxyapatite precipitate. The temperature and composition surveys that are also presented have been mapped on this yield diagram as a point (I) for temperature survey conditions and a line (II) for composition survey conditions.

The temperature survey shown in Figures 1−4 in position (c) shows phase output, theoretical output yield in moles, and equilibrium pH across the specified temperature range (25−60 °C), which brackets the range of that of the biomimetic precursor paradigm. This survey summarizes the changes in the yield diagram at a set point over a temperature range with additional quantitative yield and pH information. The precursor concentrations in all temperature surveys were conducted at 0.5/0.3 *m* (Ca/P = 1.67). The phases that are produced at 25 °C are directly shown within the corresponding phase field on the yield diagram (labeled point (I) in Figures 1−4 in position (b)).

Table 2. Relevant Chemical Equilibria for Selected Precursor Systems Used for Synthesizing Hydroxyapatite

$H_2O(l) = H^+ + OH^-$
$H_2O(g) = H_2O(l)$
$HNO_3(g) = HNO_3(aq)$
$HNO_3(aq) = H^+ + NO_3^-$
$HCl(g) = HCl(aq)$
$HCl(aq) = H^+ + Cl^-$
$Na_2HPO_4 \cdot 12H_2O(s) = 2Na^+ + HPO_4^{2-} + 12H_2O$
$Na_2HPO_4 \cdot 2H_2O(s) = 2Na^+ + HPO_4^{2-} + 2H_2O$
$Na_2O(s) + 2H^+ = 2Na^+ + H_2O$
$NaC_2H_3O_2 \cdot 3H_2O(s) = Na^+ + C_2H_3O_2^- + 3H_2O$
$NaC_2H_3O_2(aq) = Na^+ + C_2H_3O_2^-$
$NaC_2H_3O_2(s) = Na^+ + C_2H_3O_2^-$
$NaOH \cdot H_2O(s) = Na^+ + OH^- + H_2O$
$NaOH(s) = Na^+ + OH^-$
$Na_2HPO_4 \cdot 7H_2O(s) = 2Na^+ + HPO_4^{2-} + 7H_2O$
$Na_2HPO_4(s) = 2Na^+ + HPO_4^{2-}$
$Na_3PO_4 \cdot H_2O(s) = 3Na^+ + PO_4^{3-} + H_2O$
$Na_3PO_4 \cdot 6H_2O(s) = 3Na^+ + PO_4^{3-} + 6H_2O$
$Na_3PO_4 \cdot 8H_2O(s) = 3Na^+ + PO_4^{3-} + 8H_2O$
$Na_3PO_4(s) = 3Na^+ + PO_4^{3-}$
$Na_4P_2O_7 \cdot 10H_2O(s) = 4Na^+ + P_2O_7^{4-} + 10H_2O$
$Na_5P_3O_{10} \cdot 6H_2O(s) + 2OH^- = 5Na^+ + 3PO_4^{3-} + 6H_2O + 2H^+$
$Na_5P_3O_{10}(s) + 2H_2O(s) = 5Na^+ + 3PO_4^{3-} + 4H^+$
$NaH_2PO_4 \cdot H_2O(s) = Na^+ + H_2PO_4^- + H_2O$
$NaH_2PO_4 \cdot 2H_2O(s) = Na^+ + H_2PO_4^- + 2H_2O$
$NaH_2PO_4(s) = Na^+ + H_2PO_4^-$
$Na_3PO_4 \cdot 0.25NaOH \cdot 12H_2O(s) = 3.25Na^+ + PO_4^{3-} + 0.25 OH^- + 12H_2O$
$K_2HPO_4 \cdot 3H_2O(s) = 2K^+ + HPO_4^{2-} + 3H_2O$
$K_2HPO_4 \cdot 6H_2O(s) = 2K^+ + HPO_4^{2-} + 6H_2O$
$K_2HPO_4(s) = 2K^+ + HPO_4^{2-}$
$K_3PO_4 \cdot 3H_2O(s) = 3K^+ + PO_4^{3-} + 3H_2O$
$K_3PO_4 \cdot 7H_2O(s) = 3K^+ + PO_4^{3-} + 7H_2O$
$K_3PO_4(s) = 3K^+ + PO_4^{3-}$
$KH_2PO_4(s) = K^+ + H_2PO_4^-$
$KC_2H_3O_2(aq) = K^+ + C_2H_3O_2^-$
$KOH \cdot H_2O(s) = K^+ + OH^- + H_2O$
$KOH \cdot 2H_2O(s) = K^+ + OH^- + 2H_2O$
$KC_2H_3O_2(s) = K^+ + C_2H_3O_2^-$
$K_2O(s) + 2H^+ = 2K^+ + H_2O$
$KCl(aq) = K^+ + Cl^-$
$KCl(s) = K^+ + Cl^-$
$KNO_3(s) = K^+ + NO_3^-$
$KOH(s) = K^+ + OH^-$
$Ca_3(PO_4)_2(s) = 3Ca^{2+} + 2PO_4^{3-}$
$CaH_2(PO_4)_2 \cdot H_2O(s) = Ca^{2+} + 2H_2PO_4^- + H_2O$
$CaH_2(PO_4)_2(s) = Ca^{2+} + 2H_2PO_4^-$
$CaH_2PO_4^+ = Ca^{2+} + H_2PO_4^-$
$CaHPO_4 \cdot 2H_2O(s) = Ca^{2+} + HPO_4^{2-} + 2H_2O$
$CaHPO_4(aq) = Ca^{2+} + HPO_4^{2-}$
$CaHPO_4(s) = Ca^{2+} + HPO_4^{2-}$
$Ca(OH)_2(s) = Ca^{2+} + 2OH^-$
$CaOH^+ = Ca^{2+} + OH^-$
$CaPO_4^- = Ca^{2+} + PO_4^{3-}$
$CaO(s) + 2H^+ = Ca^{2+} + H_2O$
$Ca(C_2H_3O_2)_2 \cdot H_2O(s) = Ca^{2+} + 2C_2H_3O_2^- + H_2O$
$Ca(C_2H_3O_2)_2 \cdot 2H_2O(s) = Ca^{2+} + 2C_2H_3O_2^- + 2H_2O$
$Ca(C_2H_3O_2)_2(aq) = Ca^{2+} + 2C_2H_3O_2^-$
$Ca(C_2H_3O_2)_2(s) = Ca^{2+} + 2C_2H_3O_2^-$
$CaC_2H_3O_2^+ = Ca^{2+} + C_2H_3O_2^-$
$Ca_2Cl_2O \cdot 2H_2O(s) + H^+ = 2Ca^{2+} + 2Cl^- + OH^- + 2H_2O$
$CaCl_2 \cdot H_2O(s) = Ca^{2+} + 2Cl^- + H_2O$
$CaCl_2 \cdot 2H_2O(s) = Ca^{2+} + 2Cl^- + 2H_2O$
$CaCl_2 \cdot 4H_2O(s) = Ca^{2+} + 2Cl^- + 4H_2O$
$CaCl_2 \cdot 6H_2O(s) = Ca^{2+} + 2Cl^- + 6H_2O$
$CaCl_2(aq) = CaCl^+ + Cl^-$
$CaCl_2(s) = Ca^{2+} + 2Cl^-$
$CaCl^+ = Ca^{2+} + Cl^-$
$Ca(NO_3)_2 \cdot 3H_2O(s) = Ca^{2+} + 2NO_3^- + 3H_2O$
$Ca(NO_3)_2 \cdot 4H_2O(s) = Ca^{2+} + 2NO_3^- + 4H_2O$
$Ca(NO_3)_2(s) = Ca^{2+} + 2NO_3^-$
$CaNO_3^+(s) = Ca^{2+} + NO_3^-$
$Ca_8H_2(PO_4)_6 \cdot 5H_2O(s) = 8Ca^{2+} + 2H^+ + 6PO_4^{3-} + 5H_2O$
$Ca_5(PO_4)_3OH(s) = 5Ca^{2+} + 3PO_4^{3-} + OH^-$
$Ca_5(PO_4)_3Cl(s) = 5Ca^{2+} + 3PO_4^{3-} + Cl^-$
$P_2O_7^{4-} + H_2O = 2PO_4^{3-} + 2H^+$
$H_2P_2O_7^{2-} = H^+ + HP_2O_7^{3-}$
$H_2PO_4^- = H^+ + HPO_4^{2-}$
$H_3P_2O_7^- = H^+ + H_2P_2O_7^{2-}$
$H_3PO_4(aq) = H^+ + H_2PO_4^-$
$H_4P_2O_7(aq) = H^+ + H_3P_2O_7^-$
$HP_2O_7^{3-} = H^+ + P_2O_7^{4-}$
$HPO_4^{2-} = H^+ + PO_4^{3-}$
$P_4O_{10}(s) + 6H_2O = 4H_2PO_4^- + 4H^+$
$(C_2H_3O_2)_2(aq) = 2C_2H_3O_2(aq)$
$(C_2H_3O_2)_2(g) = (C_2H_3O_2)_2(aq)$
$CH_3COOH(aq) = H^+ + C_2H_3O_2^-$
$CH_3COOH(g) = CH_3COOH(aq)$

The composition survey (d) shows the phase output, theoretical yield, and pH with variable phosphate concentration (0−1 *m*) at a fixed calcium concentration (0.5 *m* unless otherwise indicated). This is a rerepresentation of the yield diagram, but with quantitative yield and pH at the set calcium concentration. The shown dominant phase changes on the composition survey are directly a result of crossing incipient precipitation boundaries on the yield diagram as labeled line (II) in Figures 1−4 in position (b).

A general way to read each set of figures is to start with the stability diagram to target the desired phase to be synthesized, in this case hydroxyapatite, and the pH/solution concentration boundaries of the phase field. For the biomimetic precursor paradigm, this would be a pH between 6.8 and 7.6. Since the stability diagram requires simulated titration of an acid and base, mentioned earlier, to generate the model, the true equilibrium solution pH can be mapped directly to the temperature survey (c) at 25 °C. Depending on precursor selection, this pH range may or may not fall within the hydroxyapatite incipient precipitation boundary on the stability diagram (a). Next, reference the yield diagram and point (I) that corresponds to the conditions modeled in temperature survey (c), taking note how far inside the phase field the fixed Ca/P precursor ratio falls. The span of precursor ratios capable of producing hydroxyapatite is a measure of process robustness; in this case, it will be measured by an estimated proportion of the yield diagram covered with a shaded 99% hydroxyapatite yield. Synthesis process robustness is important when a process is scaled up to an industrial magnitude because these processes can have some degree of experimental error for the selected precursor ratios yet still produce phase pure hydroxyapatite. Finally, referencing the composition survey (d) at the fixed 0.5 *m* calcium concentration shows and verifies the phases shown on the yield diagram along with the pH change seen as stoichiometry crosses the phase boundaries shown in the yield diagrams (Figures 1−4, position (b)) along the composition survey line (II).

2.2. Thermodynamic Models. The $CaCl_2-Na_3PO_4-H_2O$, $CaCl_2-K_2HPO_4-H_2O$, $Ca(OH)_2-H_3PO_4-H_2O$, and $Ca(C_2H_3O_2)_2-K_3PO_4-H_2O$ precursor systems are shown in Figures 1−4. The $Ca(OH)_2-K_3PO_4-H_2O$ and $Ca(OH)_2-K_2HPO_4-H_2O$ models are not presented because the final equilibrium pH of these systems was greater than 12 in both cases, eliminating them from consideration based on the biomimetic precursor paradigm.

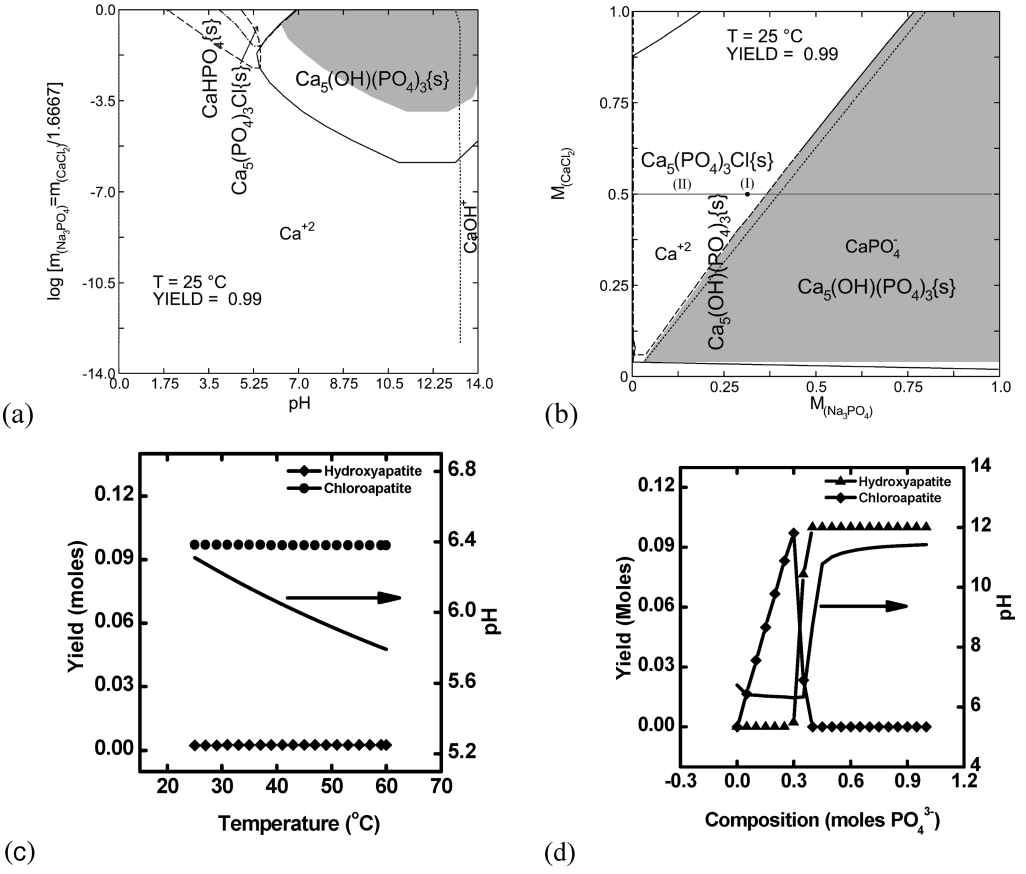

Figure 1. (a) Stability diagram (0.5 *m* $CaCl_2$, 0.3 *m* Na_3PO_4) and (b) yield diagram with corresponding (I) point and (II) line of conditions surveyed. (c) Temperature survey at 0.5 *m* $CaCl_2$ and 0.3 *m* Na_3PO_4 and (d) composition survey at 25 °C, 0.5 *m* $CaCl_2$.

The models using Na_3PO_4 are also not presented as they were close to identical to the same models presented that use K_3PO_4.

Thermodynamic evaluation of each system will be based on temperature, pH, process synthesis robustness, and yield parameters, and systems not meeting the desired parameters will be eliminated from experimental validation. The phase pure precipitation of hydroxyapatite should happen between 20 and 40 °C and a pH between 7 and 7.8 to be consistent with the biomimetic precursor paradigm. The shaded area and corresponding process synthesis robustness should cover at least half the yield diagram indicating that a large variation in composition will yield the same phase with no secondary phase contamination. Finally, the yield demonstrated in the composition survey should be at 99% yield of hydroxyapatite when the pH is in the targeted range of 7−7.8. The percent yield quoted for each system is calculated by taking the absolute moles of hydroxyapatite yielded on the composition survey when the pH is between 7 and 8 and dividing by the theoretical full yield of that system. The theoretical full yield is calculated by taking the molal quantity of calcium used in the composition diagram and dividing by five calcium ions used in each mole of hydroxyapatite ($Ca_5(PO_4)_3OH$); for most of the systems explored this is 0.5 *m*/5 = 0.1 *m*.

2.2.1. $CaCl_2$−Na_3PO_4−H_2O Equilibria System. In the $CaCl_2$−Na_3PO_4−H_2O system, two solid phases are shown to precipitate. Figure 1a shows a pH dependent precipitation of hydroxyapatite, the majority of this phase field occurring above pH 7. In the 0.5/0.3 *m* Ca/P ratio, the equilibrium pH at room temperature is about 6.2 (from Figure 1c), making chloroapatite the dominant phase under the desired conditions when temperature is between 20 and 40 °C. The yield diagram in Figure 1b shows the coprecipitation of chloroapatite and hydroxyapatite in over half the area where calcium concentrations are equal to or higher than the phosphate concentration, corresponding to conditions when the pH is lower than 10. The phase pure hydroxyapatite phase field occurs in the other half, dominantly where the system is in excess of phosphate (Ca/P < 1.67). Concentrating on these phase pure conditions in light of the biomimetic precursor paradigm, the concentration survey shows that the dominant hydroxyapatite precipitation occurs above a phosphate concentration of 0.35 *m* (calcium concentration of 0.5 *m*). This coincides with an equilibrium pH increase to over 8, which is outside the ideal biomimetic range. Precipitating very close to the single/double phase field boundary would target the pH to the proper range between 6.5 and 8; however, it would limit the robustness of the system to where the phosphate precursor concentration could not fluctuate below 0.3 *m* when the calcium precursor concentration is kept at 0.5 *m*. Additionally, when the pH is kept in this range, the yield of hydroxyapatite is 99% but a slight change in composition will

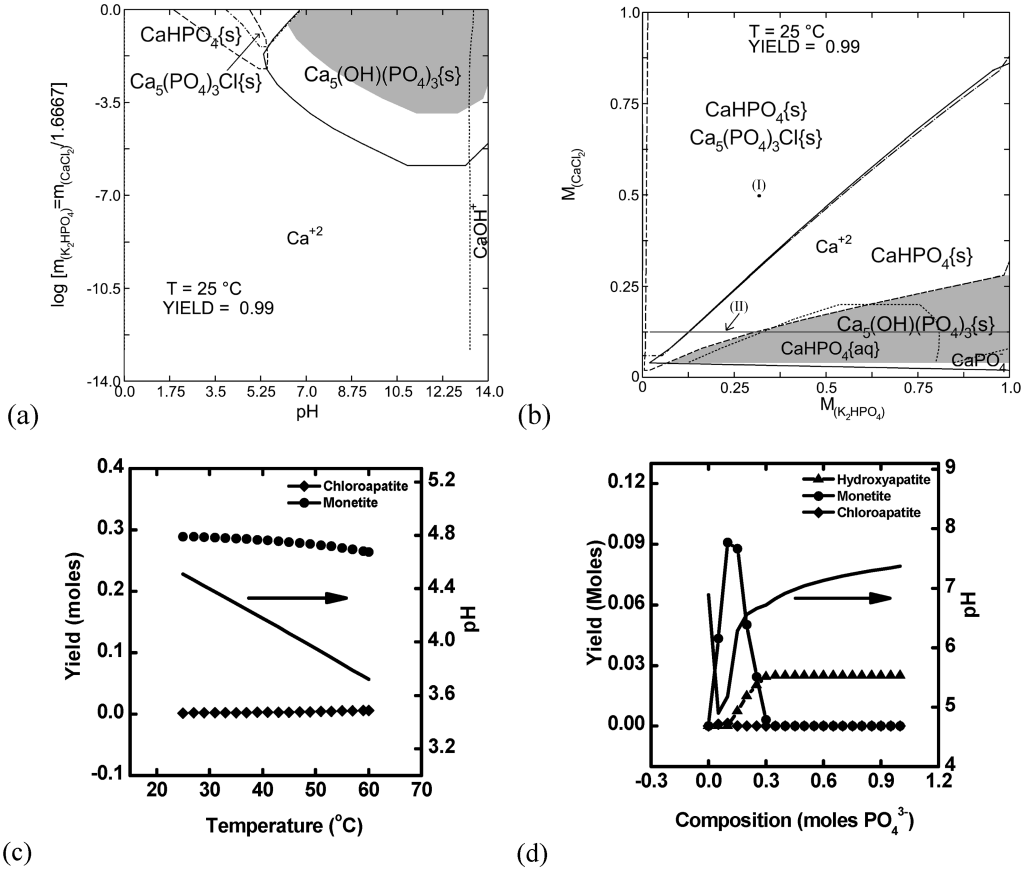

Figure 2. (a) Stability diagram (0.5 *m* $CaCl_2$, 0.3 *m* K_2HPO_4) and (b) yield diagram with corresponding (I) point and (II) line of conditions surveyed. (c) Temperature survey at 0.5 *m* $CaCl_2$ and 0.3 *m* K_2HPO_4 and (d) composition survey at 25 °C, 0.125 *m* $CaCl_2$.

precipitate chloroapatite. The calculated yield is 76% which corresponds to a calcium concentration of 0.5 *m* and a phosphate concentration of 0.35 *m* which yields a pH of 8. These secondary phase precipitation and lower yield limitations indicate this system is not a good fit for the biomimetic precursor paradigm, eliminating it as a candidate for experimental validation.

2.2.2. $CaCl_2-K_2HPO_4-H_2O$ Equilibria System. When examining the $CaCl_2-K_2HPO_4-H_2O$ models in Figure 2, it is evident that there is a limited hydroxyapatite phase stability field within this precursor system. The stability diagram in Figure 2a shows a pH dependent behavior of hydroxyapatite precipitation with an additional chloroapatite phase field coinciding with monetite between a pH of 1 and 7, whereas hydroxyapatite is phase pure above pH 7. The temperature survey (Figure 2c) for the 0.5/0.3 *m* concentration yields no hydroxyapatite over the entire 20−60 °C range due to the formation of acidic HCl species in solution driving the pH far below its stability of 6.5−12, prompting the formation of monetite and chloroapatite. The composition survey in Figure 2d conducted at 0.125 *m* $CaCl_2$, where hydroxyapatite is stable, shows an increase in equilibrium pH to values close to 7 through the use of excess phosphate above 0.34 *m*. The lower calcium concentration (0.125 *m*) used in this composition survey was chosen so the survey line on the yield diagram would intersect the hydroxyapatite phase region of interest. The yield diagram in Figure 2b further emphasizes the limited stoichiometry ranges for the synthesis of phase pure hydroxyapatite showing only a small shaded region (~20% of the total area) when the precursor system is kept in extreme excess of phosphate ($Ca/P \ll 1.67$, $Ca < 0.2$ *m*, $PO_4 > 0.25$ *m*). The resulting robustness of this system is very low, only producing high yield phase pure hydroxyapatite in a small range of stoichiometries. At these stoichiometries, the yield is 99%, which corresponds to a calcium precursor concentration of 0.125 *m* and phosphate precursor concentration of 0.5 *m*, producing a pH of 7. Note how far the temperature survey point (I) is away from the hydroxyapatite phase stability region, emphasizing how drastically the stoichiometry has to be changed to yield the targeted phase. The low robustness of the system alone eliminates this as a candidate for further experimental investigation.

2.2.3. $Ca(OH)_2-H_3PO_4-H_2O$ Equilibria System. Moving away from chloride based chemistries, the investigation of the $Ca(OH)_2-H_3PO_4-H_2O$ system (Figure 3) yields a different set of thermodynamic issues when looking for precursor systems to fit the paradigm. The stability diagram in Figure 3a shows the same pH dependent behavior seen in the previous models indicating this phenomenon is not unique to the precursor systems employed. In each of the three systems explored so far, the shaded region dimensions span from pH of about 6.5 to 14 and $\log[m_{(PO4)} = m_{(Ca)}/1.6667]$ of −4.2 to 0. There is a change in the shape of the secondary monetite phase field, showing an overlap and coprecipitation with hydroxyapatite around a pH of 5.25.

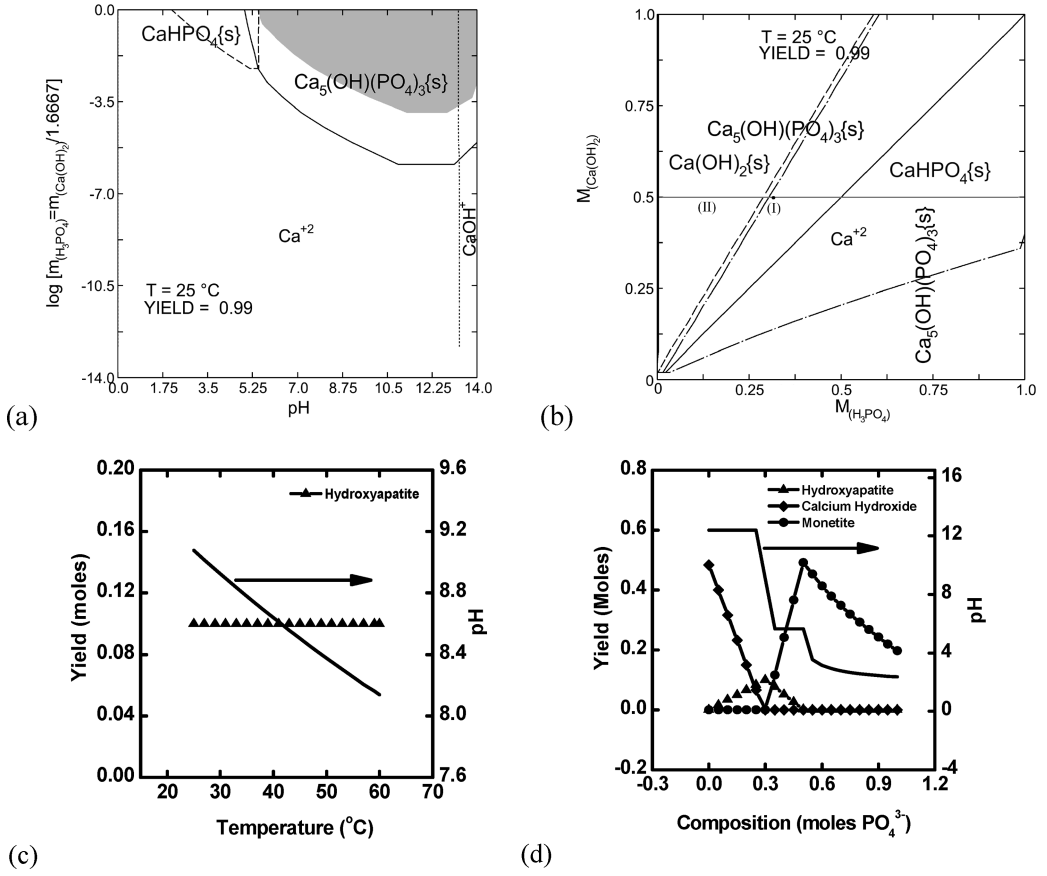

Figure 3. (a) Stability diagram (0.5 *m* $Ca(OH)_2$, 0.3 *m* H_3PO_4) and (b) yield diagram with corresponding (I) point and (II) line of conditions surveyed. (c) Temperature survey at 0.5 *m* $Ca(OH)_2$ and 0.3 *m* H_3PO_4 and (d) composition survey at 25 °C, 0.5 *m* $Ca(OH)_2$.

The yield diagram in Figure 3b indicates no area where hydroxyapatite is the only dominant phase at 99% yield, simply because this precursor system has a Ca/P ratio of 1.6667 that falls just outside the shaded region adjacent to the monetite field on the stability diagram. When calculating percent yield from the composition survey, however, it is found that 99% yield may exist with a calcium precursor inflow of 0.5 *m* and phosphate precursor inflow of 0.3 *m* corresponding to a pH of 8. However, any deviation away from this phosphate precursor concentration will coprecipitate an undesired phase. The small triangular area where temperature survey point (I) is located on the yield diagram in Figure 3b yields hydroxyapatite as the only phase precipitated; however, it is obvious this system is very sensitive to precursor ratio changes. A shift of Ca/P above 1.75 or below 1.0 will yield a coprecipitation field, severely limiting the robustness of this system and carrying it outside the desired pH range. Although hydroxyapatite is the dominant phase at 0.5/0.3 *m* over the entire temperature range of 20−60 °C in Figure 3c, the equilibrium pH, is 9.1, which is above the range for the paradigm. However, looking at the composition survey, using a slight excess of phosphate (Ca/P = 1.55−1.65) may serve to target the initial pH in the biological range of 7.1−7.6, but this range must be maintained throughout synthesis so as not to precipitate secondary phases in this narrow region of targeted phase stability. On the basis of low yield and lack of robustness when in accordance to the biomimetic precursor paradigm, this system was eliminated from experimental validation.

2.2.4. $Ca(C_2H_3O_2)_2-K_3PO_4-H_2O$ Equilibria System. In the previously unexplored $Ca(C_2H_3O_2)_2-K_3PO_4-H_2O$ system shown in Figure 4, some different thermodynamic characteristics are observed. The stability diagram shows the same pH sensitivity as the other chemistries explored; however, it appears to have a slightly more narrow pH region starting at 7 rather than around 6.5, so further analysis was done to see how the shaded 99% yield phase field may move when stoichiometry is altered (Ca/P = 1.47−1.6833) in this system. As shown in Figure 5a, the shaded hydroxyapatite precipitation region recedes with a decrease in the phosphate precursor concentration (increase in Ca/P ratio), the largest area being with an excess of phosphate at the 1.47 Ca/P ratio, or 0.34 *m* K_3PO_4. It is likely that this receding phenomenon is also seen in the other chemistries as well. The yield diagram in Figure 4b shows a protruding monetite phase field and its recession with higher temperatures, being completely eliminated by 40 °C. It is predicted that even inside this phase field hydroxyapatite will be a dominant coprecipitate, making this the only diagram explored that can yield hydroxyapatite over the entire range of precursor ratios (Ca = 0.001−1 *m*, PO_4 = 0.001−1 *m*). Using an excess of phosphate or an excess of calcium will yield phase pure hydroxyapatite outside this

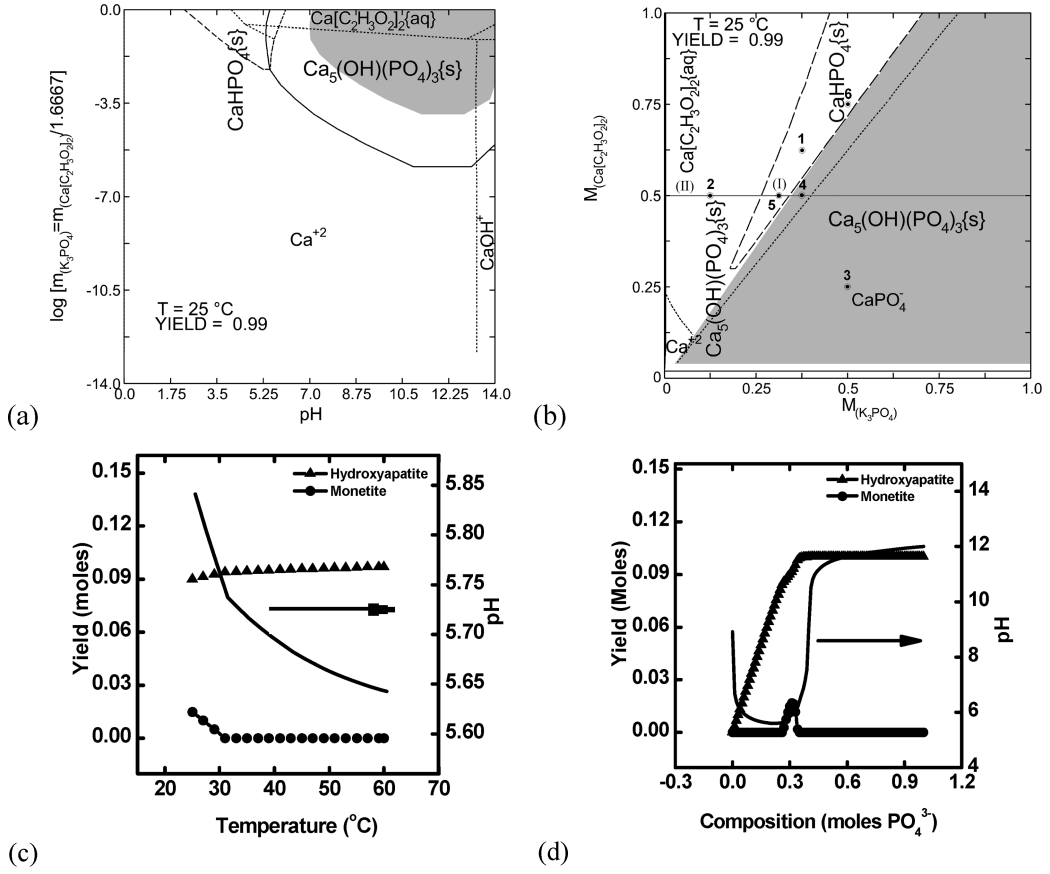

Figure 4. (a) Stability diagram (0.5 *m* $Ca(C_2H_3O_2)_2$, 0.3 *m* K_3PO_4) and (b) yield diagram with corresponding (I) point and (II) line of conditions surveyed and 1−6 points of validation. (c) Temperature survey at 0.5 *m* $Ca(C_2H_3O_2)_2$ and 0.3 *m* K_3PO_4 and (d) composition survey at 25 °C, 0.5 *m* $Ca(C_2H_3O_2)_2$.

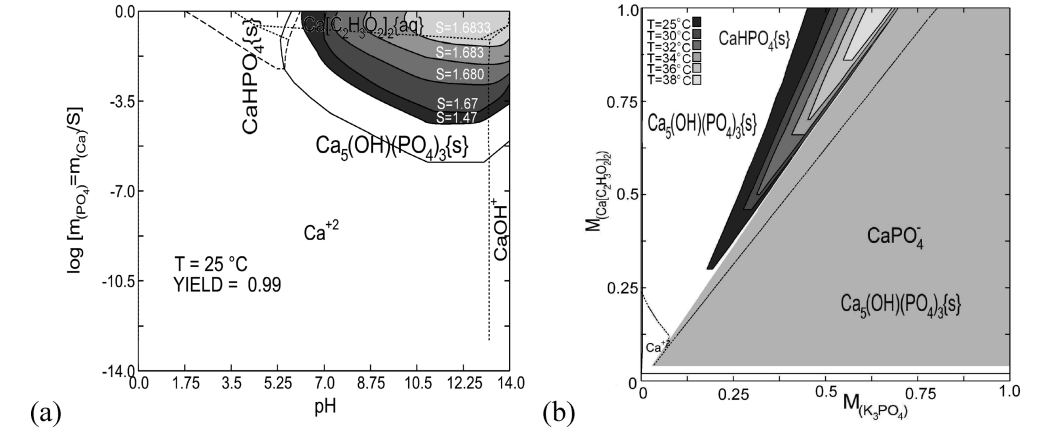

Figure 5. (a) Stability diagram with corresponding adjustments in stoichiometry and its effects on 99% yield area and (b) yield diagram at 37 °C.

monetite coprecipitation field; however, only an excess of phosphate will produce 99% yield and reach the targeted biomimetic pH range (mapped from Figure 4d). When the same model is calculated at 37 °C (Figure 5b), the monetite phase field retracts to a very small area produced at high concentrations of precursors. The 0.5/0.3 *m* temperature survey indicates that hydroxyapatite is not phase pure at room temperature, but by 31 °C, it is the dominant precipitate. The equilibrium pH is low for the application to a biological system, but the compositional survey indicates that the increase of phosphate concentration to 0.39 *m* raises the equilibrium pH to 7.5 and produces phase pure hydroxyapatite at 99% yield. The robustness of the system could be considered comparable to that of the $CaCl_2-Na_3PO_4-H_2O$ system; however, crossing out of the 99% yield shaded region in a phosphate-deficient formulation when the temperature is brought up to 37 °C, hydroxyapatite is still a phase pure precipitate, giving this system an advantage. Even when compared at 25 °C, the area of the monetite phase field in this system is much smaller to design around than the coprecipitating chloroapatite phase field in the $CaCl_2-Na_3PO_4-H_2O$ precursor system. Given the advantages in robustness and the smaller secondary

Table 3. Summary of Six Reaction Conditions Chosen from Figure 4d

sample ID	computed Ca/P ratio	calcium SS (m)	phosphate SS (m)	post-mixing Ca/P concentrations (*m*)
1	1.67	1.25	0.75	0.625/0.375
2	4.00	1.00	0.25	0.500/0.125
3	0.50	0.50	1.00	0.250/0.500
4	1.33	1.00	0.75	0.500/0.375
5	1.67	1.00	0.60	0.500/0.300
6	1.50	1.50	1.50	0.750/0.500

coprecipitation phase field, this system was chosen for experimental model validation.

3. Experimental Validation

3.1. Procedure. Six points were chosen on the diagram presented in Figure 4b, three within the monetite phase field, and three at other stoichiometries within the predicted phase pure hydroxyapatite field within and outside the region of 99% yield. The synthesis of the powder was carried out using calcium acetate hydrate (99%, Acros Organics, Morris Plains, NJ) and potassium phosphate tribasic monohydrate (96%, Acros Organics, Morris Plains, NJ) as received with no further purification or treatment. The concentrations of the precursor solutions tested are presented in Table 3 and are expressed in premixing concentrations. For example, an experimental 1.0 *m* solution of calcium acetate would be 0.5 *m* after mixing (hereto referred to as a post-mixing concentration) with a corresponding equal volume phosphate solution. A stock solution (SS) of calcium acetate and a separate stock solution of potassium phosphate tribasic were made by dissolving the appropriate amount of precursor in DI water (deionized water, Milli-Q biocell with RiOs-S, Millipore Systems, Inc., Billerica, MA) and filtering through a 0.2 μm PES membrane Nalgene filter (566-0020). An equal volume (50 mL) of each solution was measured out, and the phosphate solution was added to the calcium solution. The resulting viscous liquid was then stirred vigorously until the solution formed thixotropic gel turned white and reduced in viscosity in about 30 s of mixing. This solution was aged for 4 h, centrifuged (Avanti J-26XP, Beckman Coulter, Fullerton, CA), washed (where indicated with 150 mL DI water each cycle), shell frozen (Labconco, Kansas City, MO), freeze-dried (Dura-Dry μP, FTS Systems, Inc., Stone Ridge, NY), and desiccated (Drykeeper, Sanplatec Corp, Osaka, Japan, humidity 30%) until ready for characterization. Powders that were fired were subjected to a 900 °C heat treatment for 2 h in air to verify complete reaction of the precursors and reagent concentrations (2 h ramp to 900 °C, 2 h hold, 6 h ramp down).

Processing pH was measured versus reaction time for 1−4 h (Table 4) for comparison to predicted equilibrium pH at the various Ca/P stoichiometries. It was notable that even after 4 h, none of the Ca/P stoichiometries had pH values that fell as low as the predicted equilibrium pH in Table 4. For example, sample 5 was computed to have an equilibrium pH of 5.8 while the experimental pH after a 4 h reaction time was 9.0. Thus, these data indicate that

Table 4. Measured pH of Samples 1−6 as a Function of Reaction Time, Post-Wash pH after 2 Washing Cycles, and Computed Equilibrium pH

	Sample ID					
time (h)	1	2	3	4	5	6
0	11.0	9.5	14.0	10.0	11.0	12.0
1	9.5	9.0	14.0	10.0	9.0	9.5
2	9.5	8.5	14.0	10.0	9.0	9.5
3	9.0	7.2	14.0	9.5	9.0	9.5
4	8.5	7.2	14.0	9.5	9.0	9.0
post-wash (2 cycles)	6.9	< 6.5	12.0	7.2	6.9	6.9
equilibrium pH	5.9	5.8	12.0	7.2	5.8	6.2

at the end time of synthesis the systems shown in Table 4 were still approaching equilibrium.

When the precipitate was washed, the pH was noticed to decrease by 2 ± 0.5 pH points compared to prewashing. On the basis of these results, when it is important to ensure phase purity in future studies, pH during post-synthesis processing should be closely monitored or the powder should be washed in buffered solutions to prevent the formation of undesired phases. The pH of the residual washing medium after the powder has been centrifuged out is described as "pH after washing." The sample nomenclature used is as follows: as-prepared (AP), as-prepared heat treated (APHT), as-prepared washed (APW), and as-prepared washed and heat treated (APWHT).

3.2. Characterization. Reaction products for the $Ca(C_2H_3O_2)_2-K_3PO_4-H_2O$ system were characterized via X-ray diffraction (XRD) (Kristalloflex D-500, Siemens Analytical X-ray Instruments, Madison, WI., 30 mA, 40 kV, Cu Kα, 2-theta = 20−60°, 0.03 step, 2 s dwell). Jade 8.0 Software (MDI, Livermore, CA) was used to aid in phase identification with PDF numbers 01-074-0566 (hydroxyapatite), 01-077-0128 (monetite), 97-002-2239 (calcium potassium phosphate (V) alpha), 01-070-0364 (M tricalcium phosphate, α-TCP), and 01-070-2065 (R tricalcium phosphate, β-TCP).

3.3. Results and Analysis. The results of the XRD validation are presented in Figures 6 and 7. The as-synthesized powders in both the washed and the unwashed conditions (Figures 6a, 7a) yielded hydroxyapatite as the dominant phase in most cases. Looking at each of the six points tested, three were predicted to produce phase pure hydroxyapatite (points 2−4) and three were predicted to produce hydroxyapatite and monetite coprecipitate (points 1, 5−6). All as-prepared powder produced hydroxyapatite as predicted but only AP6 produced monetite as predicted (2-theta = 26.6°). What appeared inconsistent with the diagrams were the final pHs of the as-prepared powders, possibly suggesting that there is a kinetic time component that plays an integral part, as the pHs were significantly higher than predicted, but the reaction was stopped at 4 h, long before equilibrium was reached. AP2, although with a starting pH of 9.5, higher than the paradigm allows, was the only stoichiometry experimentally investigated that seemed to fit the biomimetic model post-synthesis (pH = 7.2)

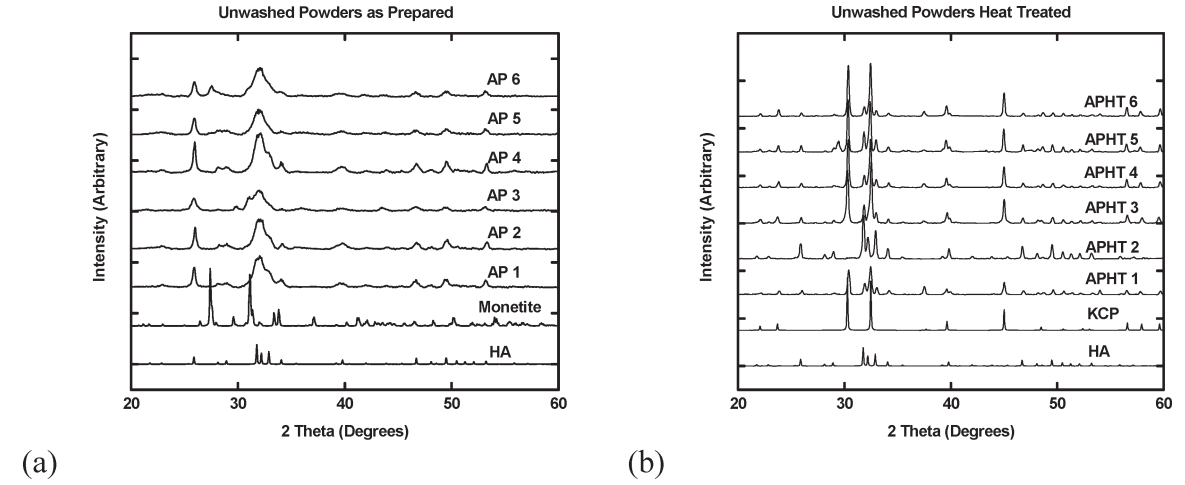

Figure 6. XRD of (a) unwashed powders as-synthesized and (b) unwashed heat treated powders showing a phase development of calcium potassium phosphate(V) alpha.

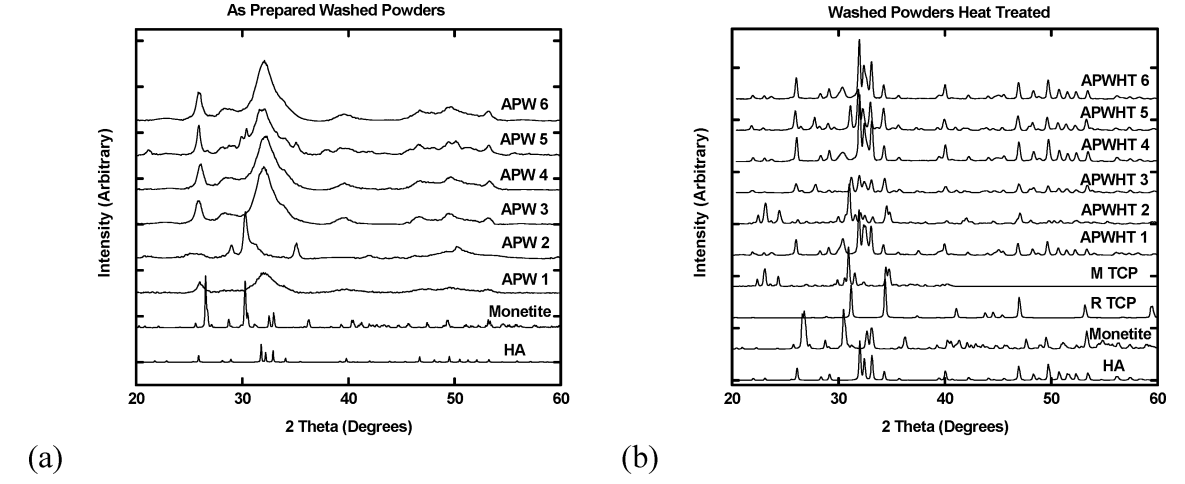

Figure 7. XRD of (a) washed powders and (b) washed and heat treated powders demonstrating sensitive secondary phase developments that heavily rely upon washing treatments.

without the use of washing, additives, or buffers. With the use of an even more calcium-rich ratio, it may have an even lower starting pH (targeted in the range of 7.4) and a shorter reaction time, although a smaller yield, being outside the 99% shaded region.

Although the final synthesis pHs are still above the desired target, it is notable that 1−2 washing cycles diluting the synthesis liquid threefold was enough to bring the pH of all but one system down to the targeted pH range of 7−7.8. In comparison, the other chemical systems modeled in this study utilize more extreme pH conditions, requiring a minimum of three washing cycles that dilute the synthesis liquid volume by up to 10-fold each time. The lower volumes of severe washing conditions used for the acetate system give it a considerable advantage over other precursor systems for large scale production of hydroxyapatite, since fewer washes and lower volumes of washing media are required. The only unexpected result was that after washing, APW2, an extremely phosphate-deficient formulation, was converted into monetite. This result was consistent with pH/phase predictions in the stability diagram, associated with the solution pH dropping below 6.5 in the post-washing step shown in Table 4. This suggests it is imperative to monitor and control pH within the pH stability range of hydroxyapatite while washing these powders to maintain these powders as hydroxyapatite. It is useful to note that the model-predicted synthesis of hydroxyapatite over the selected regions of the equilibrium diagram did hold true, emphasizing that this chemistry has a much higher degree of robustness than any previously explored.

To determine the presence of incomplete crystallization and nonstoichiometric hydroxyapatite, heat treatments of 900 °C for 2 h were done on both washed and unwashed powders to observe any high temperature phase development. Upon heat treating the AP powders, all phases transformed into dominantly calcium potassium phosphate (V) alpha (KCP) with a small amount of hydroxyapatite except AP2, which remained hydroxyapatite with no detectable secondary phases, indicating this calcium rich ratio produces stoichiometric HA, while the others are all nonstoichiometric. KCP is phase predicted to form at high temperatures in traditional

ternary and binary diagrams using a calcium and phosphate source with a potassium component.[48] It can be speculated that leaving the potassium ions on the surface of the particles adjusted the phase stability of hydroxyapatite at high temperatures, prompting the crystal structure to incorporate a significant potassium contingent but remain hexagonal. Hydroxyapatite is known to incorporate large amounts of impurities, so it is expected with higher rates of diffusion at this high temperature for this phase to develop. It would be interesting to see if a different cation doped calcium phosphate phase develops at high temperature when using an alternative tribasic phosphate source such as sodium orthophosphate or ammonium orthophosphate. Moreover, since tricalcium phosphate was not formed, it can be speculated that there was no amorphous phase left at the end of reaction. Two brief washing cycles with DI water (Figure 7a-b) purged the system of potassium preventing any calcium potassium phosphate development upon heat treatment. There was an exception, however, with the previously mentioned monetite that developed in APW2 due to a pH drop, which caused a transformation upon firing into dominantly monoclinic α-TCP. The APW5 did, however, develop a small quantity of monetite or amorphous calcium phosphate during or following the washing cycles, which appears to have converted into a small amount of hexagonal β-TCP with firing (2-theta = 30.7°). The other APWHTs appear to have some small degree of phase transformation to β-TCP and/or monetite, but a considerable portion of these samples remained hydroxyapatite, even upon heat treatment. The amounts of monetite seen in the APWHTs can be likely ascribed to the second washing cycle causing a drop in pH into the metastable range below 7.

(48) *ACerS-NIST phase Equilibria Diagrams* [CD-ROM], version 3.0.1; 2004.

4. Conclusions

Thermodynamic computations were effectively used to evaluate four important precursor systems for the synthesis of hydroxyapatite using biomimetic precursor design criteria. They were also effective in discovering processing conditions suitable for hydroxyapatite synthesis using calcium acetate and potassium orthophosphate. The calcium acetate−potassium orthophosphate system demonstrated the most robust processing conditions and has the ability to synthesize hydroxyapatite over the entire range of Ca/P stoichiometries explored. The pH dependence and 99% yield behavior demonstrated in the stability diagrams for all four precursor systems appears to be universal with respect to precursor choice when single calcium and single phosphate precursors are employed at a stoichiometric ratio of Ca/P = 1.6667.

Acknowledgment. The authors would like to acknowledge NASA GSRP Grant NNG04GO44H, the Rutgers-NSF IGERT DGE 0333196, and Osteotech, Inc., for their generous funding of this research.